Torque Dense, External Rotor Hub-Drive for a Hybrid Solar Vehicle

R. Wrobel[1], N. McNeill[1], D.A. Staton[2], J.D. Booker[1], P.H. Mellor[1]
[1]Faculty of Engineering, University of Bristol, Bristol, BS8 1UB, UK
[2]Motor Design Ltd, Shropshire, SY12 9DA, UK
Email: p.h.mellor@bristol.ac.uk

***Abstract* – This paper considers the design of an open-slot, external-rotor radial-flux brushless permanent motor based upon a single-layer concentrated 'modular' winding. The magnetic circuit design of the most promising pole-slot combinations has been optimised using a procedure comprising a genetic algorithm coupled to a parametric finite element model. The best combinations of pole and slot numbers are presented for which the torque per volume is maximal and torque ripple is minimal. The outcome of the research has been applied to the design of a prototype 24-slot 28-pole motor configured as wheel hub drive for use in a hybrid solar assisted bicycle. The attributes of the design are assessed using test results obtained from this purpose built hub-motor.**

I. Introduction

There are many automotive applications where a direct drive torque dense electrical machine is highly desirable. Examples include wheel hub drives for electric vehicles and starter-generators integrated within engines. The most common configurations of direct drive motors are either radial field external rotor or axial-flux topologies [1–4].

This paper describes a configuration for an open-slot, external-rotor radial-flux brushless permanent motor, based on a single-layer concentrated 'modular' winding [1–3]. Compared against a conventional 1.5 slots/pole concentrated winding, the modular winding approach potentially has a superior electromagnetic and thermal performance whilst retaining a compact end-winding with minimal overhang. An aim of the research has been to quantify these benefits.

Employing an open slot stator lamination greatly simplifies manufacture since it allows the stator coils to be preformed and inserted onto the stator teeth. With a preformed coil a compact and consistent winding lay is possible and high copper fill factors are readily achieved. The use of an open slot is normally associated with high levels of cogging and torque ripple. With the modular winding these effects can be minimised through an appropriate selection of pole and slot number.

Fig. 1 shows the prototype hub-motor used in the investigation integrated within a 20 inch diameter bicycle wheel. The design torque rating of this machine is 8 Nm. The intended application of this traction drive is in a hybrid solar vehicle which is under development for entry into the 2007 World Solar Cycle Challenge. An analytical lumped parameter thermal model of the machine has also been developed to appraise its thermal performance.

Fig. 1. Prototype external-rotor motor fitted within a wheel- hub

II. Electromagnetic Design

A number of authors have investigated the best combination of the pole and slot numbers for modular wound machines [1–3]. Table I presents candidate pole-slot combinations for which the winding factor is greatest (0.966). This value is 11% larger than the equivalent winding factor of a standard 1.5 slots-per-pole configuration (0.866). Also included in the Table is the least common multiple (LCM) index that indicates the number of cogging torque periods per rotor revolution. The higher values of LCM occur at higher pole numbers and correspond to the lowest cogging torque.

TABLE I

Winding Factor and LCM for Different Pole Slot Combinations

	Motor version	k_w	LCM
1)	$p = 10, q = 12$	0.966	60
2)	$p = 14, q = 12$	0.966	84
3)	$p = 20, q = 24$	0.966	120
4)	$p = 28, q = 24$	0.966	168
5)	$p = 30, q = 36$	0.966	180
6)	$p = 42, q = 36$	0.966	252

A detailed evaluation of the six pole-slot combinations listed in Table I has been undertaken [5]. In each case a genetic algorithm (GA) coupled to parametric two-dimensional magneto-static FE model was employed to optimise magnetic design in order to determine the configuration that yields maximum torque density. These candidate motor versions are characterised by the same total slot area available for the winding and by equal volume of permanent magnet.

The availability of auto-meshing parametric FE solvers [6] coupled with rapid advances in computational power provides opportunities to employ numerical optimisation techniques within a non-linear FE model. The general optimisation problem can be defined in *n*-dimensional calculation space where *n* is equal to the number of optimised parameters. The solution of the problem is given as a set of parameters $\mathbf{x} = \{x_1, x_2, \ldots, x_n\}$ for which an objective function $f(\mathbf{x})$ has a maximal or minimal value. A genetic algorithm (GA) [7] searches the solution space of a function using simulated evolution, where the parameter set $\mathbf{x}$ is often referred to as a chromosome.

To simulate the evolution process the combination of the three basic operators: selection, crossover and mutation, are used in the GA. In general, the fittest individuals of any population tend to reproduce and survive to the next generation, thus improving successive generations. However, inferior individuals are also able to reproduce [8]. In this case the GA is used to determine the magnetic circuit configuration that will yield maximum torque. The objective function is therefore:

$$f(\mathbf{x}) = \max_{\mathbf{x} \in \Re^n} \left(T_j(\mathbf{x}) \right) \tag{1}$$

where $T_j(\mathbf{x})$ is the electromagnetic torque for a single set of design parameters $\mathbf{x}$ (chromosome). To emulate brushless DC operation the FE model is evaluated at a number of rotor positions over an electrical cycle and averaged over successive 60° electrical commutations of the winding current pattern. The operation of the machine is assumed to be ideal with constant magnitude phase currents that change instantaneously at each commutation event. The torque is calculated using the co-energy method.

Four variables were considered in the formulation of the chromosome $\mathbf{x}$ and the parametric FE model: the outer diameter of the stator lamination, the depth of the rotor back iron, the tooth width, and the depth of slot. The remaining attributes of the design were constrained as follows:

- the outer diameter (120mm);
- the cross section areas of permanent magnet (1.0×10^{-3} m^2) and slots (2.4×10^{-3} m^2);
- the peak fundamental component of the magnetic flux density in the stator core and rotor back iron (1.5 T);
- the width of the air-gap (1 mm);
- the winding current density (4.5 A/mm^2 referenced to the slot area).

The permanent magnets are fully pitched and diametrically magnetised and formed from a 38MGOe grade of sintered NdFeB.

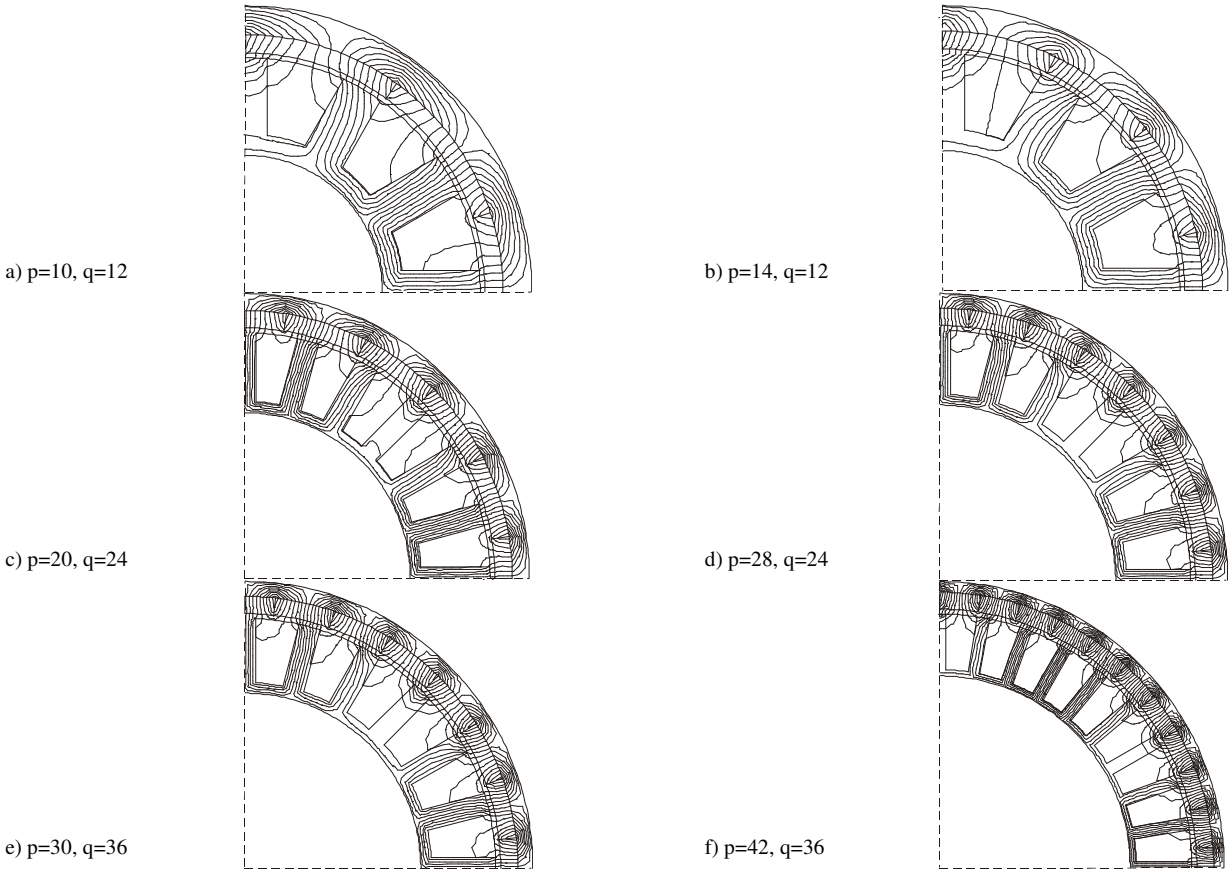

Fig. 2 Optimised designs of the six motor configurations showing the no-load magnet flux contours

The six GA optimised motor structures together with no-load contour plots of the magnetic flux density are presented in Fig. 2.

TABLE II
SPECIFIC TORQUE OF THE VARIOUS MOTOR CONFIGURATIONS

Motor version		T_{av}/V [kNm/m^3]
1)	$p = 10$, $q = 12$	23.4
2)	$p = 14$, $q = 12$	26.5
3)	$p = 20$, $q = 24$	29.8
4)	$p = 28$, $q = 24$	30.9
5)	$p = 30$, $q = 36$	32.2
6)	$p = 42$, $q = 36$	31.0

Table II compares the torque per unit volume of each optimised design. The volume factor used in these calculations is the total volume of active materials, comprising the stator laminations and back iron, the copper and the permanent magnets, along the active length of the motor. Of the versions considered the highest torque per volume is obtained with motor version 5. However the trend would suggest there is little advantage in using a very high pole number particularly when other factors such as stator iron loss and eddy current losses in the permanent magnets are taken into account. Whilst the quoted torque density figures are based on an idealised brushless DC motor operation the values are comparable with the best direct-drive motor topologies [8]

III. PROTOTYPE DIRECT DRIVE HUB MOTOR

The 28 pole, 24 slot configuration (version 4) was chosen for prototyping on the basis of having a good torque density and a manageable number of parts for manufacture.

A major feature of the design lies in the open slot stator lamination design that allows pre-forming of the stator coils. Fig. 3 shows a section through a pre-formed stator coil which has been vacuum impregnated with high thermal conductivity varnish. Through this manufacturing technique a copper fill factor exceeding 60% is easily achieved.

The stator lamination pack was formed from bonded 0.35mm Si-Fe laminations and heat shrunk onto a hollow axel. The twelve preformed coils are then bonded onto the stator lamination pack and their connecting wires routed through the hollow shaft assembly. In the prototype all of the coil ends were externally available to enable different connection arrangements for test purposes. In addition a number of thermocouples were buried in the slots and attached to the coil end-turns and the stator iron.

The rotor was constructed from standard rectangular blocks of permanent magnet mounted to a single piece back-iron machined from magnetically permeable steel, Fig. 5. Whilst magnet eddy current losses in the magnet array and rotor iron losses are likely to be high with this topology, this loss is readily dissipated via the wheel hub.

The combined weight of the stator and rotor assemblies is 2.2 kg.

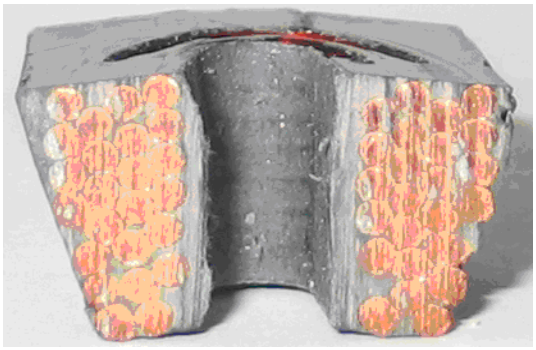

Fig. 3. Section through an individual impregnated coil indicating a high copper fill factor

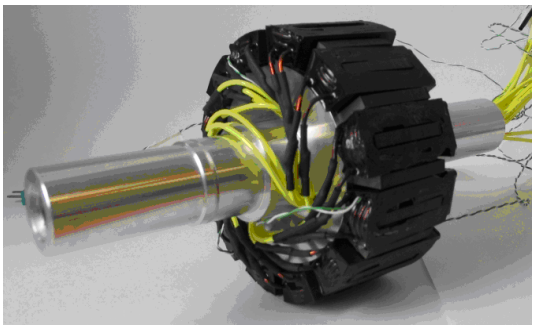

Fig. 4. Preformed coils positioned onto the stator core and axel

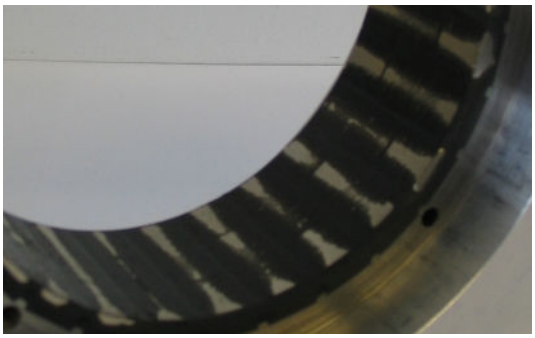

Fig. 5. Rotor construction

IV. ELECTROMAGNETIC TESTS

Initially the motor was tested to confirm the electromagnetic predictions. The wheel was mounted onto a test rig comprising a roller connected to a DC load machine, Fig 6. The wheel assembly was mounted on gimbals and the reaction torque measured via a load cell.

Fig. 7 compares the measured emf waveform with the FE predictions. As would be expected they are in good agreement, the differences being attributed to tolerances in the permanent magnet properties and construction. The peak value of cogging torque was measured to be 50 mNm, confirming the low expected value.

A particular attribute of modular windings is the low mutual coupling between individual coils or phases, a feature which can be exploited to provide fault tolerance [9]. Table III gives the range of measured values of self- and mutual-inductance for the twelve stator coils. The mutual coupling between the coils varies between 8% and 10%.

TABLE III
MEASURED INDIVIDUAL COIL SELF AND MUTUAL INDUCTANCES

Self-inductance		Mutual-inductance	
Max.	Min.	Max.	Min.
62 mH	58 mH	5.4 mH	4.8 mH

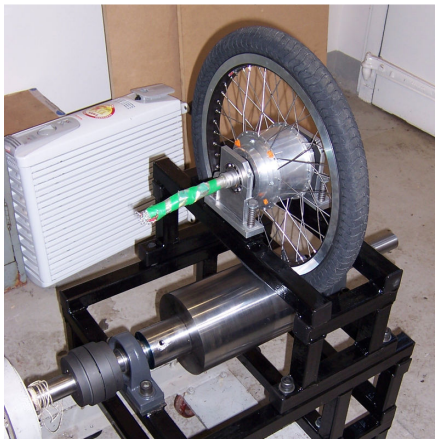

Fig. 6. 'Rolling road' test arrangement

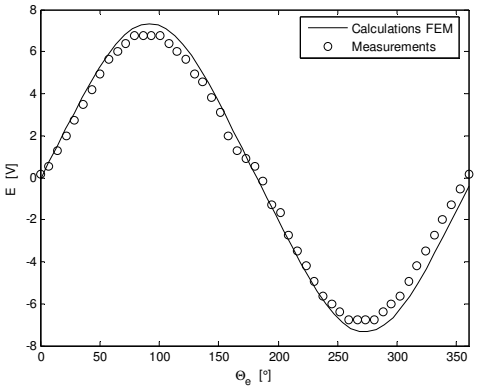

Fig. 7. Measured and FE calculated emf waveform (250 rpm)

Load tests were undertaken with the motor driven at a constant speed of 250 rpm from a MOSFET Brushless DC controller. These results are summarised in Table IV. The measured torque constant is comparable to the finite element analysis prediction of 0.54 Nm/A_{rms} assuming ideal operation. At high torques the losses are dominated by winding copper loss resulting in a relatively low efficiency. With this topology the rotor loss is also significant and was estimated to be around 15 W at the 10 Nm, 250 rpm load point. Despite the reduced efficiency the motor is able to run continuously at 10 Nm output.

TABLE IV
250 rpm LOAD TEST RESULTS

Torque [Nm]	Phase current [A_{rms}]	Torque constant [Nm/A_{rms}]	Efficiency [%]
3.6	7.5	0.48	81
4.4	8.8	0.50	81
6.3	12.2	0.51	75
7.6	14.7	0.52	70
10.1	19.3	0.52	64

V. THERMAL MODEL AND ASSESSMENT

A lumped-parameter thermal model has been developed for the machine to investigate potential heat transfer benefits of the construction. This custom model was implemented within a commercial thermal analysis software package [10]. Due to the relatively short stack length of the machine, the heat transfer in both the radial and axial direction is considered. Fig. 8 indicates the main constituent elements of the model; the hub, the rotor iron, the magnets, the stator, the winding, the shaft, the bearings and endcaps.

Lumped thermal resistances model the main heat transfer paths and cater for heat conduction, convection and radiation. A schematic view of the thermal resistance network used for the motor is shown in Fig. 9. A total of 27 temperature nodes were used corresponding to various elements of the winding, stator yoke and teeth, permanent magnets, rotor back iron, etc. The colours in the schematic correspond to the different materials used in the motor construction, Fig. 8. A thermal resistance marked with a C denotes a heat transfer via convection whilst an R denotes heat radiation. Resistances shown in two colours represent the interface between two components. These interface resistances can be a major contribution to the temperature rise of the machine [11].

Losses, indicated as a current source symbol in the network schematic, are injected at appropriate nodes corresponding to the windings, the iron and the permanent magnets. The circuit is then solved for the temperatures at each node. The transient thermal behaviour can be estimated by adding thermal capacitances to the circuit nodes. In traction applications this transient performance is significant since it can dictate the maximum acceleration or regenerative braking capabilities of the vehicle.

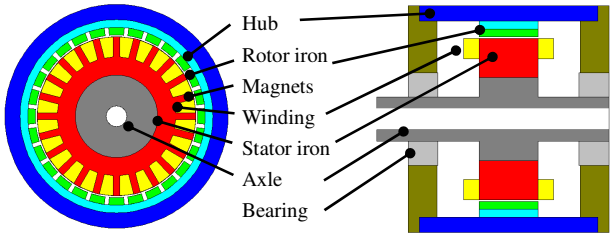

Fig. 8. Radial and axial sections used in formulating the thermal model

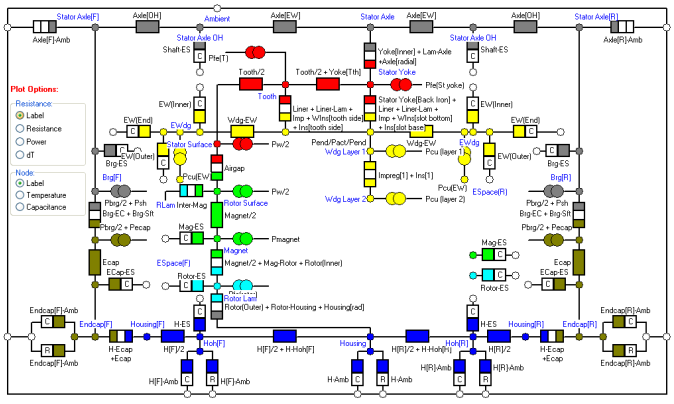

Fig. 9. Thermal resistance network

The steady state temperatures of the shaft, end-winding and external hub have been measured at 250 rpm for a number of different loads. Estimates of losses in the copper, iron, permanent magnets, and bearings are then put into the thermal model at the appropriate nodes. The copper loss was determined from the winding resistance which was adjusted to account for the temperature variation of copper resistivity. The iron losses were estimated from lamination material properties using an embedded model within the FE solver. These values were multiplied by a 1.5 build factor to account for the effect of the stator manufacture. The bearing losses were taken from the manufacturer's data. Finally the rotor loss was estimated from the difference between the total measured loss and the sum of the other components.

A comparison between the measured and predicted temperatures is given in Table V. In the predictions the thermal resistance of the axle mounting arrangement on the test bed has been calibrated to the measured axle temperatures. The thermal model provides a good estimate of the winding and hub temperatures.

TABLE V
MEASURED AND PREDICTED MOTOR TEMPERATURES

Phase current [A_{rms}]	Measured			Predicted		
	Winding (1) [°C]	Axle(2) [°C]	Hub [°C]	Winding (3) [°C]	Axle (2) [°C]	Hub [°C]
8	56	46	-	53	44	42
15	103	72	-	108	72	66
19	145	95	87	156	94	86

Notes (1) – maximum measured temperature
(2) – average axial temperature
(3) – peak predicted temperature in the centre of the slot

The thermal model was employed to provide an initial assessment of the thermal advantage of the modular winding over the more conventional 1.5 slot per pole design. An equivalent thermal model for a 12-slot, 18-pole design was constructed with the same principal dimensions. The cross section of this machine is shown in Fig. 10. Initial results from this study indicate the winding temperature rise is around 15% higher in the conventional machine for the same slot fill and copper loss. Further work is required in order to undertake a fairer and more detailed comparison taking into account the difference design attributes of the two machine topologies.

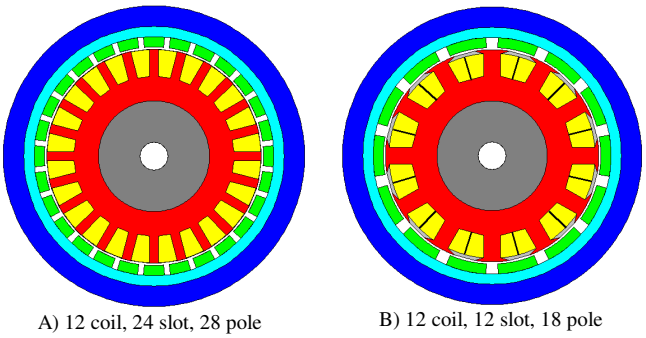

A) 12 coil, 24 slot, 28 pole B) 12 coil, 12 slot, 18 pole

Fig. 15. Cross sections used in the thermal comparisons.

V. CONCLUSIONS

The paper has presented a design for an external-rotor torque dense brushless PM motor. The use of a 'modular' single-layer concentrated winding combined with an open-slot stator construction allows the use of preformed stator coils to realise a high copper fill factor and a compact end-winding with minimal overhang. The arrangement also results in a superior conductive heat transfer between the winding and the stator axel assembly. Good heat transfer from the winding is critical as the internal mounting of the stator means the windings are remote from any cooling air. Furthermore the dominant loss in the motor is winding copper loss.

A 24-slot, 28-pole version has been prototyped and demonstrated as a wheel-hub drive. Test results from this machine have demonstrated the following attributes:

- A continuous torque rating exceeding 10Nm. At 10Nm output the equivalent torque density is 37kNm/m^3 and 4.5 Nm/kg. This calculation is based upon the combined volume/weight of the stator and rotor assemblies.
- Low cogging torque and torque ripple despite the open slot stator lamination construction
- Superior thermal performance compared to conventional 1.5 slot/pole concentrated windings

A single-layer concentrated wound machine would be expected to have high eddy current losses in the rotor. However this loss was not significant in the prototype despite the use of a non-laminated back-iron and standard permanent magnet blocks. As the rotor assembly is integral to the wheel-hub any rotor loss is readily dissipated.

REFERENCES

[1] J. Cros, P. Viarouge, "Synthesis of high performance pm motors with concentrated windings", *IEEE Trans. Energy Conversion*, 2002, 17, 248-253.

[2] J. D. Ede, K. Atallah, J. B. Wang, D. Howe, "Modular fault-tolerant permanent magnet brushless machines", *IEE Proceedings on Power Electronics, Machines and Drives*, 2002, 415-420.

[3] F. Magussen, C. Sadarangani, "Winding factor on Joule losses of permanent magnet machines with concentrated windings", *IEEE Int. Electric Machines and Drives Conference IEMDC'03,* 2003, 1, 333-339.

[4] M. Łukaniszyn, R. Wróbel, "A Study on the Influence of Permanent Magnet Dimensions and Stator Core Structures on the Torque of the Disc-Type Brushless DC Motor," *Electrical Engineering*, 2000, 82, 163-171.

[5] R. Wobel, P. H. Mellor, "Design Considerations of a Direct Drive Brushless Machine with Concentrated Windings", *IEEE Int. Electric Machines & Drives Conference IEMDC'05*, San Antonio, USA, 2005, 655-658.

[6] D. Meeker, Finite Element Method Magnetics Version 3.2 User's Manual, 2002.

[7] C.R. Houck, J. A. Joines, and M. G. Kay, 'A genetic algorithm for function optimization: A Matlab implementation', *NCSU-IE Technical Report 95-09*, 1995.

[8] Y. Chen, P. Pillay, A. Khan, 'PM wind generator topologies', *IEEE Transactions on Industry Applications*, 2005, 41(6), 1619-1626.

[9] B.C. Mecrow, A.G. Jack, J.A. Haylock, J. Coles, 'Fault-tolerant permanent magnet machine drives', IEE Proc.B ,1996, 143(6), 437-442

[10] Motor-CAD v3.1 software manual, April 2006.

[11] D.A. Staton, A. Boglietti, A., Cavagnino, 'Solving the More Difficult Aspects of Electric Motor Thermal Analysis in Small and Medium Size Industrial Induction Motors'; *IEEE Transactions on Energy Conversion*, 2005, 20(3), 620–628.